

# High-Motility Visible Light-Driven Ag/AgCl Janus Micromotors

Xu Wang, Larysa Baraban,\* Anh Nguyen, Jin Ge, Vyacheslav R. Misko, Jacques Tempere, Franco Nori, Petr Formanek, Tao Huang, Gianauelio Cuniberti, Jürgen Fassbender, and Denys Makarov\*

Visible light-driven nano/micromotors are promising candidates for biomedical and environmental applications. This study demonstrates blue light-driven Ag/AgCl-based spherical Janus micromotors, which couple plasmonic light absorption with the photochemical decomposition of AgCl. These micromotors reveal high motility in pure water, i.e., mean squared displacements (MSD) reaching  $800 \mu\text{m}^2$  within 8 s, which is 100× higher compared to previous visible light-driven Janus micromotors and 7× higher than reported ultraviolet (UV) light-driven AgCl micromotors. In addition to providing design rules to realize efficient Janus micromotors, the complex dynamics revealed by individual and assemblies of Janus motors is investigated experimentally and in simulations. The effect of suppressed rotational diffusion is focused on, compared to UV light-driven AgCl micromotors, as a reason for this remarkable increase of the MSD. Moreover, this study demonstrates the potential of using visible light-driven plasmonic Ag/AgCl-based Janus micromotors in human saliva, phosphate-buffered saline solution, the most common isotonic buffer that mimics the environment of human body fluids, and Rhodamine B solution, which is a typical polluted dye for demonstrations of photocatalytic environmental remediation. This new knowledge is useful for designing visible light driven nano/micromotors based on the surface plasmon resonance effect and their applications in assays relevant for biomedical and ecological sciences.

fundamentals<sup>[1]</sup> to real-life applications.<sup>[2]</sup> Pioneering studies on the propulsion of different objects (e.g., tubular,<sup>[3]</sup> helical,<sup>[4]</sup> gear,<sup>[5]</sup> rod-like,<sup>[6]</sup> and Janus particles<sup>[4b,7]</sup>) allowed for the determination of the fundamental mechanisms of motion<sup>[2a,8]</sup> and highlighted a number of promising applications, especially in environmental research,<sup>[2b]</sup> biology, and medicine.<sup>[2c,9]</sup> Furthermore, for these synthetic motors to achieve deterministic motion over large distances, distinct mechanisms have already been explored, including bubble propulsion,<sup>[9d,10]</sup> electrophoresis,<sup>[3b,6a,11]</sup> ultrasonic wave actuation,<sup>[12]</sup> AC and DC magnetic field actuation,<sup>[13]</sup> and diffusiophoresis.<sup>[14]</sup> For applications in a physiological environment or environmental remediation, the propulsion mechanism should be properly selected to fulfill a number of stringent requirements, including usage of low toxicity solutions, being easily controllable, and allowing for high-speed movement.

Currently, one of the most active research directions is the realization of

light-driven nano/micromotors using different light sources.<sup>[15]</sup> The light is used to either initiate thermophoretic propulsion of the particles<sup>[5a,16]</sup> or activate and control a photocatalytic reaction.<sup>[17]</sup> Typically, lasers (with wavelength  $\lambda = 808 \text{ nm}$ )<sup>[18]</sup> and ultraviolet (UV) ( $\lambda = 340\text{--}380 \text{ nm}$ )<sup>[19]</sup> radiation are applied. To

## 1. Introduction

The research field of man-made nano/micromotors is growing significantly at the level of new materials and fabrication, as well as numerous exciting demonstrations, ranging from

X. Wang, Dr. J. Ge, Prof. J. Fassbender, Dr. D. Makarov  
Helmholtz-Zentrum Dresden-Rossendorf e.V.  
Institute of Ion Beam Physics and Materials Research  
Bautzner Landstrasse 400, 01328 Dresden, Germany  
E-mail: d.makarov@hzdr.de

Dr. L. Baraban, A. Nguyen, T. Huang, Prof. G. Cuniberti  
Institute for Materials Science and Max Bergmann  
Center of Biomaterials  
Technische Universität Dresden  
01062 Dresden, Germany  
E-mail: larysa.baraban@nano.tu-dresden.de

Dr. L. Baraban, T. Huang, Prof. G. Cuniberti  
Center for Advancing Electronics Dresden  
Technische Universität Dresden  
01062 Dresden, Germany

 The ORCID identification number(s) for the author(s) of this article can be found under <https://doi.org/10.1002/sml.201803613>.

DOI: 10.1002/sml.201803613

Dr. V. R. Misko, Prof. J. Tempere  
Theory of Quantum and Complex Systems Laboratory  
Universiteit Antwerpen  
Universiteitsplein 1, B-2610 Antwerpen, Belgium

Dr. V. R. Misko, Prof. F. Nori  
Theoretical Quantum Physics Laboratory  
RIKEN Cluster for Pioneering Research  
Wako-shi, Saitama 351-0198, Japan

Prof. J. Tempere  
Lyman Laboratory of Physics  
Harvard University  
Cambridge, MA 02138, USA

Prof. F. Nori  
Physics Department  
University of Michigan  
Ann Arbor, MI 48109-1040, USA

Dr. P. Formanek  
Leibniz-Institut für Polymerforschung Dresden e.V.  
Hohe Str. 6, 01069 Dresden, Germany

efficiently use solar energy and avoid the harmful influence to a human body for potential therapeutic applications.<sup>[20]</sup> visible light ( $\lambda = 390\text{--}700\text{ nm}$ ) has been suggested as a promising stimulus to propel nano/micromotors.<sup>[21]</sup> There is intense activity regarding the realization of visible light-controlled self-propelled micromotors in  $\text{H}_2\text{O}_2$  solution.<sup>[20,22]</sup> Only very recently, visible light was successfully applied to stimulate a directional motion in pure  $\text{H}_2\text{O}$  using Au/black  $\text{TiO}_2$  (high velocity can be achieved in  $\text{H}_2\text{O}_2$  solution),<sup>[7e]</sup> BiOI/Au (high velocity can be achieved in  $\text{H}_2\text{O}_2$  solution),<sup>[23]</sup> and Si–Au<sup>[24]</sup> composites. Certain advantage in terms of achieving high speed motion could be offered by AgCl, one of the most efficient photocatalysts, which can absorb efficiently in the UV spectral range.<sup>[25]</sup> Microparticles of AgCl of different shapes, e.g., uniform  $2\text{ }\mu\text{m}$  particles<sup>[26]</sup> and  $2\text{ }\mu\text{m}$  large microstars<sup>[27]</sup> have been used as artificial swimmers. The motion of individual particles as well as their collective behavior leading to clustering, local pumping, and schooling<sup>[26,28]</sup> is already well documented. Interestingly, due to the use of bulky and heavy AgCl microparticles, the obtained mean squared displacement (MSD) values are rather low in pure  $\text{H}_2\text{O}$ : typically in the range of up to about  $100\text{ }\mu\text{m}^2$  in 8 s despite favorable UV light illumination.<sup>[27]</sup> This is a drawback of using UV light driven AgCl-based micromotors, particularly for applications where the efficient transport of particles within bio-organisms, like blood vessels, is imperative. Plasmonic photocatalysts are typically applied to enhance the absorption ability in the visible spectral range.<sup>[25a,29]</sup> Recently, this concept was applied in the field of nanomotors,<sup>[21]</sup> where enhanced Brownian motion was successfully demonstrated in pure  $\text{H}_2\text{O}$  under visible light illumination.

Here, we demonstrate for the first time Ag/AgCl-based spherical Janus motors that reveal efficient propulsion when illuminated by visible light. Our micromotors have strong absorption ability in the visible light range ( $>420\text{ nm}$ ), because of the surface plasmon resonance (SPR) effect between AgCl nanoparticles and plasmonic Ag layer. We show that a proper design of Ag/AgCl-based micromotors can boost the MSD to a remarkable value of  $800\text{ }\mu\text{m}^2$  in 8 s in pure  $\text{H}_2\text{O}$ , even when activated using blue light (excitation  $\lambda = 450\text{--}490\text{ nm}$ , light intensity of about  $100\text{ }\mu\text{W mm}^{-2}$ ). To achieve this performance, we applied several key modifications to the type and structure of a micromotor. First, instead of AgCl microparticles with a relatively smooth surface, we use polystyrene (PS) microparticles with a cap structure formed of a rough layer of Ag/AgCl nanoparticles. Those assure a high surface-to-volume ratio, a strong light confinement effect and enhance the speed of the photocatalytic reaction. Furthermore, the rotational diffusion coefficient of a  $2\text{ }\mu\text{m}$  large polystyrene sphere is  $D_R \approx 0.165\text{ rad}^2\text{ s}^{-1}$ , which is about  $5\times$  smaller than for the previously reported AgCl micromotors.<sup>[27]</sup> This effect together with a much more efficient photocatalytic reaction is the key ingredient, which allows the Ag/AgCl-based Janus micromotors to obtain large velocities and displacements. In this work, we investigate—experimentally and using numerical simulations—the motion of individual Janus particles as well as their small (2- and 3-particle) and large (many-particle) clusters. We numerically solve the Langevin equations<sup>[30]</sup> of motion for self-propelled Janus particles using molecular-dynamics simulations. We analyze the trajectories and MSD of single Janus particles, their small “molecules” (consisting of two or three active particles), and

large clusters and compared the obtained results with the experimental observations. We experimentally demonstrate the motion of Ag/AgCl-based Janus micromotors in physiological environments under visible light illumination, such as in human saliva, phosphate-buffered saline (PBS) buffer, and Rhodamine B (RhB) aqueous solutions of different concentrations.

## 2. Results

AgCl has a weak absorption in the visible spectral range due to its large bandgaps ( $5.15\text{ eV}$  direct bandgap and  $3.25\text{ eV}$  indirect bandgap).<sup>[31]</sup> Instead, Ag/AgCl composites have strong absorption in the visible and near infrared (NIR) regions because of the coupling to the SPR of Ag.<sup>[25a,29f,32]</sup> We realize plasmonic PS/Ag/AgCl-based micromotors as follows: a monolayer of PS spherical particles with a diameter of  $2\text{ }\mu\text{m}$  is prepared by drop casting  $600\text{ }\mu\text{L}$  of ethanol-based colloidal suspension onto a round glass slide. After drying, the sample is introduced in a vacuum chamber where electron beam deposition is used to fabricate a  $60\text{ nm}$  thin Ag coating on the top surface of PS particles. The scanning electron microscopy (SEM) image of the sample after the deposition of Ag layer is shown in **Figure 1a**. We note that at the top of a cap, the surface of the Ag layer remains smooth. Closer to the equator (starting from the angular position of about  $75^\circ$  from the symmetry axis of the capped particle), we observe a grainy film morphology. To transform the Ag layer into Ag/AgCl, the sample is oxidized using a  $\text{FeCl}_3/\text{PVP}$  (polyvinylpyrrolidone) solution.<sup>[32b,33]</sup> After the in situ oxidation reaction, the original smooth surface of Ag layer is turned to a grainy layer consisting of Ag/AgCl nanoparticles with a characteristic size of  $50\text{--}100\text{ nm}$  (**Figure 1b**). The use of a highly concentrated PVP solution is crucial for promoting the formation of large Ag/AgCl clusters, stabilizing the oxidation process of Ag and resulting in a layer of Ag/AgCl.<sup>[32b]</sup> Different arrangements of Janus spheres are observed after the sample drying process, ranging from individual particles (**Figure 1c**) through their small clusters (**Figure 1d,e**) to clusters with large numbers of Janus particles. The Ag (**Figure 1f**) and Cl (**Figure 1g**) distributions over Ag/AgCl caps of Janus micromotors are shown by the energy dispersive X-ray spectroscopy (EDX) mapping. To investigate the distribution of the metallic Ag in Ag/AgCl caps, we removed the AgCl layer by mixing the PS/Ag/AgCl micromotors with an ammonium hydroxide solution ( $\text{NH}_4\text{OH}$ ). This assures that only Ag remains at the cap of the Janus particles. An SEM image of the  $\text{NH}_4\text{OH}$  processed Janus PS/Ag/AgCl particles and the corresponding EDX mapping of Ag and Cl are shown in **Figure 1h–j**, respectively. The UV–vis spectrum (**Figure 1k**) reveals the absorption peak at around  $340\text{ nm}$  for both PS/Ag and  $\text{NH}_4\text{OH}$  processed PS/Ag/AgCl Janus particles. For PS/Ag/AgCl capped spheres, the absorption peak is shifted to around  $410\text{ nm}$ . Furthermore, this sample shows efficient absorption not only in the visible but even in the NIR range because of the SPR effect, in line with previous reports on plasmonic Ag/AgCl photocatalysts.<sup>[25a,29f]</sup>

**Figure 1l** shows the schematic photocatalysis process and motion direction of a single PS/Ag/AgCl Janus micromotor. The mechanism of photoexcitation in Ag/AgCl bilayers is studied in great detail elsewhere.<sup>[29f,34]</sup> For the discussion

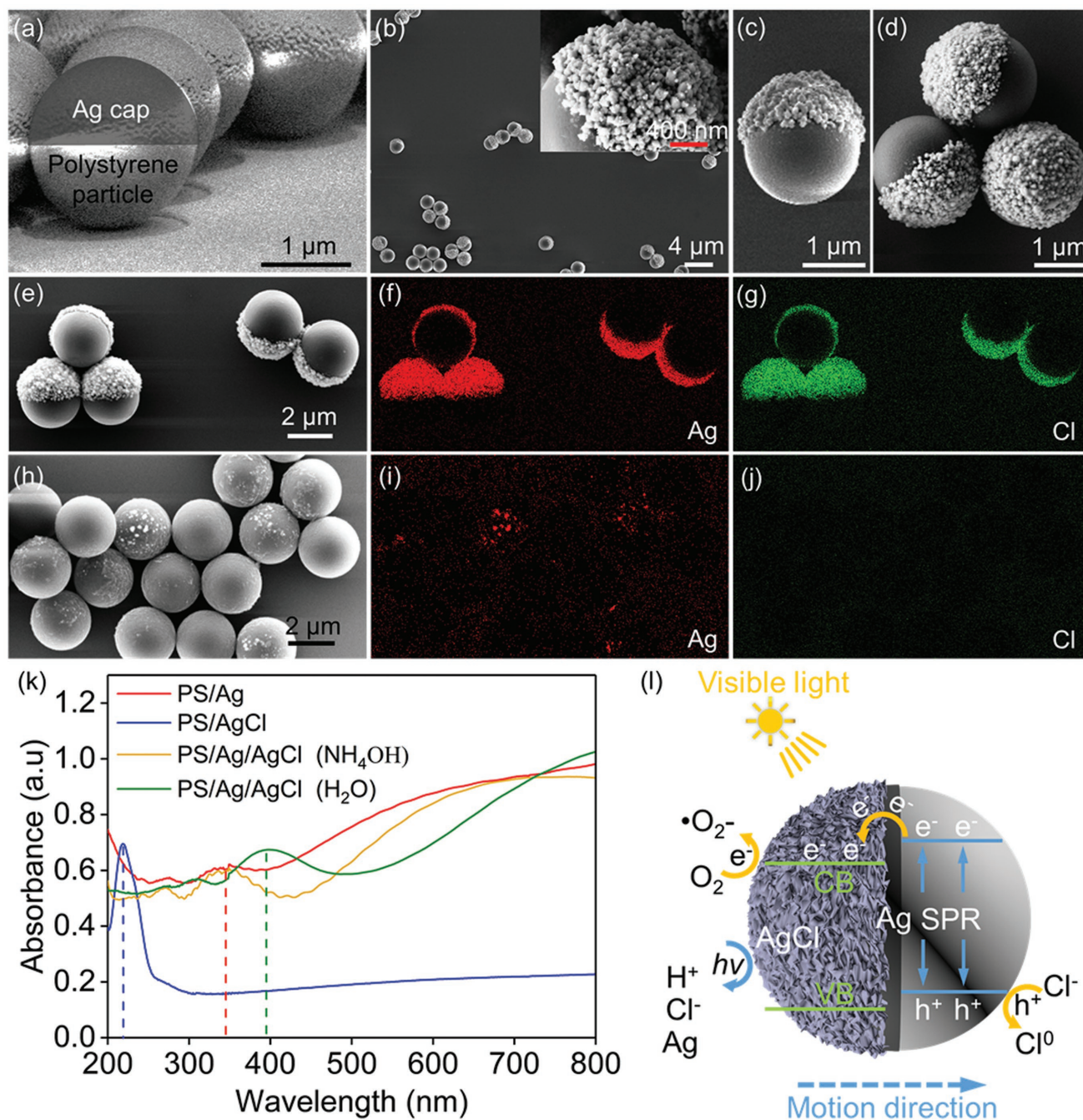


**Figure 1.** Scanning electron microscopy (SEM) images of a) as prepared PS/Ag capped particles, b) PS/Ag/AgCl Janus particle assemblies. The inset in panel (b) shows a high-resolution SEM image of the Ag/AgCl surface. Zoom on a location with c) a single Janus particle, d) cluster of 3-Janus particles, and e) clusters of 2- and 3-Janus particles. The EDX mapping of f) Ag and g) Cl elements for the sample shown in panel (e). h) SEM image of PS/Ag/AgCl Janus particles processed in ammonia solution and the corresponding EDX mapping of i) Ag and j) Cl elements. k) UV-vis absorption spectra of PS/Ag (red curve), PS/pure AgCl (blue curve), PS/Ag/AgCl (green curve), and ammonia solution processed PS/Ag/AgCl (orange curve). l) Schematic image for visible light absorption process of Janus PS/Ag/AgCl micromotors based on the SPR effect. Our model of the visible light actuated motion based on the photodecomposition process of AgCl layer is shown as well (CB: conductive band, VB: valence band).

below, it is relevant that the different diffusion speeds of H<sup>+</sup> and Cl<sup>-</sup> ions, which are provided by the photodecomposition process of AgCl, induce an asymmetric internal electric field around a Janus micromotor. Due to this fact, the motion is triggered toward the noncapped PS face.<sup>[25b]</sup> The propulsion of

micromotors in deionized (DI) water is due to the photocatalytic reduction of AgCl<sup>[35]</sup> at the location of the cap



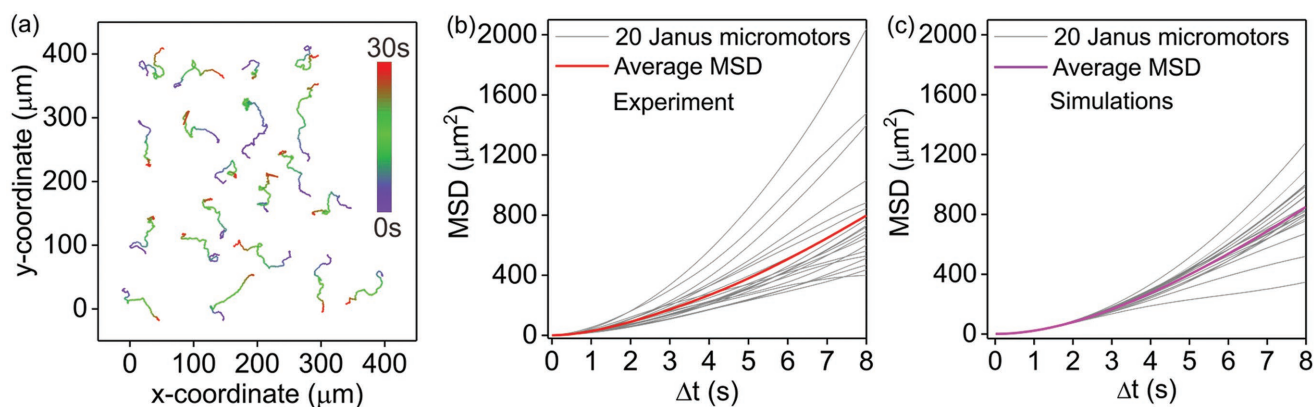


**Figure 2.** a) Trajectories of 20 single Janus PS/Ag/AgCl particles taken over 30 s under blue light illumination  $[(106 \pm 1) \mu\text{W mm}^{-2}]$ . b) The individual (grey) and averaged (red) experimental MSD curves of 20 single Janus particles. c) Representative individual (grey) and averaged (magenta) simulated MSD curves of 20 single Janus particles.

### 2.1. Dynamics of a Single Janus Particle

To obtain a quantitative insight into the dynamics of individual Janus spheres when illuminated by blue light (450–490 nm) of high intensity, we investigate the motion trajectories of 20 particles over a period of up to 30 s (Figure 2a; Video S1, Supporting Information). The trajectories are color coded to indicate the time progression while tracking. For reference, a typical Brownian motion of a Janus particle under a reference green light illumination of low intensity (see the Experimental Section) is shown in Figure 3a (Video S1, Supporting Information). Following the classical works on the evaluation of MSD,<sup>[36]</sup> we present the MSD data up to 8 s only based on the information obtained from each 30 s long tracking movie. This provides a sufficient sampling for calculating the MSD for each particle. Then, the average is taken over all the particles to obtain the resulting MSD. The MSDs for 20 particles are shown in panel (b) with gray lines. The final MSD curve,

averaged over 20 particles, is shown in red. The resulting MSD reaches remarkably high values of up to  $800 \mu\text{m}^2$  after 8 s. Note that the MSD curves for individual particles noticeably disperse around this average value and can reach values as high as about  $2000 \mu\text{m}^2$  in 8 s.

The analysis of the experimental data shown in Figure 2b is done by fitting the experimental MSD to the theoretical MSD curve<sup>[7f]</sup>

$$\text{MSD}(t) = (4D_T + v^2\tau_R)t + v^2\tau_R^2 \left[ \exp(-2t/\tau_R) - 1 \right] / 2 \quad (2)$$

In this way, we extract the effective translational  $D_{\text{eff}} = D_T + v^2/(4D_R)$  and rotational diffusion  $D_R$  coefficients. Note that for self-propelled particles,  $D_{\text{eff}}$  is mainly determined by the second term:  $v^2/(4D_R) \gg D_T$ . Therefore, we extract  $v$  and  $D_R$  from the fitting, and we use the theoretical value for the translational diffusion coefficient of a spherical pure Brownian particle of the same size as the Janus particle:

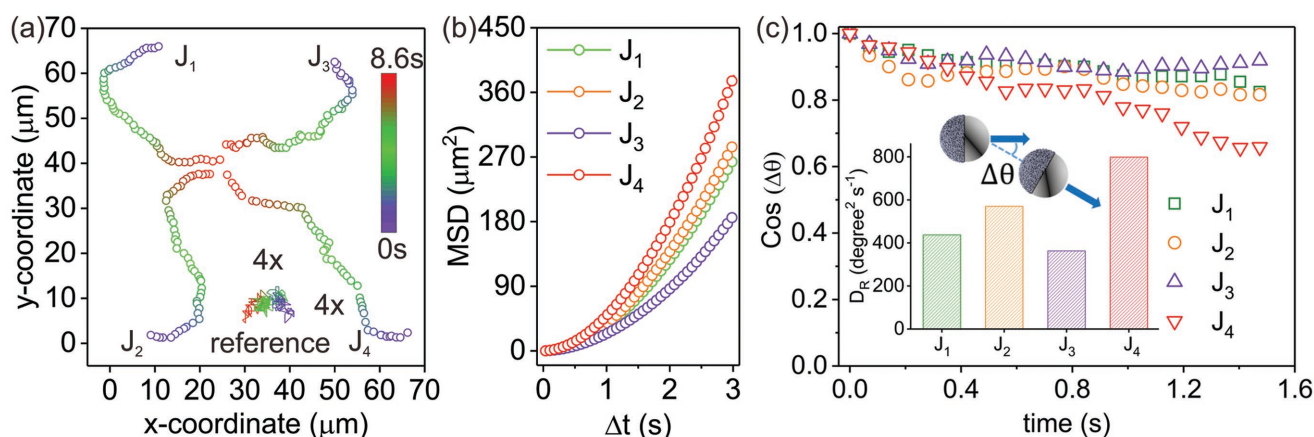


**Figure 3.** a) Trajectories of four single Janus PS/Ag/AgCl particles ( $J_1$ – $J_4$ ) taken over 8.6 s under blue light illumination  $[(106 \pm 1) \mu\text{W mm}^{-2}]$ . The trajectory of a reference Janus PS/Ag/AgCl particle under green light illumination  $[(8 \pm 1) \mu\text{W mm}^{-2}]$  is shown as well (Video S1, Supporting Information). b) The experimental MSD curves of single Janus particles:  $J_1$  ( $1193 \mu\text{m}^2$ , green symbols),  $J_2$  ( $1460 \mu\text{m}^2$ , orange symbols),  $J_3$  ( $940 \mu\text{m}^2$ , purple symbols), and  $J_4$  ( $2899 \mu\text{m}^2$ , red symbols) (Video S1, Supporting Information). c) Time evolution of the experimental autocorrelation values,  $\text{Cos}(\Delta\theta)$ , of the angle  $\Delta\theta$ , capturing the change of the orientation of the main symmetry axis of the metallic cap of a colloid between two neighboring frames in the tracking video files for the single Janus PS/Ag/AgCl particles ( $J_1$ – $J_4$ ). The upper inset shows schematics on how the angle  $\Delta\theta$  is defined. The lower inset summarizes the rotational diffusion coefficients,  $D_R$ , for four single Janus particles (Video S2, Supporting Information).

$D_T \approx 0.22 \mu\text{m}^2 \text{s}^{-1}$ .<sup>[37]</sup> The extracted average self-propulsion velocity and rotational diffusion coefficients are  $v = 4.9 \mu\text{m s}^{-1}$  and  $D_R = 0.165 \text{rad}^2 \text{s}^{-1}$ . Note that the extracted rotational diffusion coefficient is in quantitative agreement with the analytical estimate for a spherical particle:  $D_{R,A} = 0.16 \text{rad}^2 \text{s}^{-1}$  in pure water.<sup>[37]</sup> These experimentally determined values are adopted for performing molecular-dynamics simulations.

A similar trend is captured in the simulations for particles characterized by the self-propulsion velocities and the rotational diffusion coefficients:  $v = 4.9 \mu\text{m s}^{-1}$ ;  $D_R = 0.165 \text{rad}^2 \text{s}^{-1}$  and  $v = 5 \mu\text{m s}^{-1}$ ;  $D_R = 0.16 \text{rad}^2 \text{s}^{-1}$  (both the  $(v, D_R)$  sets providing good fits to the experimental MSD) (Figure 2c). We note that the values of the MSD achieved in our experiments are much higher than those reported for the AgCl star-shaped micromotors.<sup>[27]</sup> We attribute this fact to the more efficient propulsion due to the grainy morphology of AgCl films and much smaller rotational diffusion coefficient compared to the case of AgCl microstars.<sup>[27]</sup>

In addition, we also use an alternative approach to extract the rotational diffusion coefficient of single Janus particles by calculating the difference of orientation angles of the main symmetry axis of the metallic cap of a colloid between two consecutive frames (as illustrated in a schematic image, inset in Figure 3) from the tracking videos (Video S1, Supporting Information). Relevant tracking trajectories taken over 8 s are shown in Figure 3a. The calculated MSD based on the experimental tracking data over 1.5 s is shown in Figure 3b. Following the established method,<sup>[3c]</sup> we plot the mean squared angular displacement (MSAD) as a function of time. The rotational diffusion coefficient ( $D_R$ , inset in Figure 3c) is calculated based on the equation,  $\text{MSAD} = 2D_R\Delta t$ . To reveal the details of the rotational motion, we measure the variable angular value ( $\Delta\theta$ ) of Janus micromotors compared to their initial orientation and plot the autocorrelation values ( $\cos(\Delta\theta)$ ) during the initial 1.5 s (Figure 3c). The autocorrelation is decreased to a value ranging from 0.65 to 0.91, and their effective translational diffusion coefficient  $D_{T,\text{eff}} = (4D_T + v^2\tau_R)$  and rotational diffusion coefficient  $D_R$  are, respectively,  $65 \mu\text{m}^2 \text{s}^{-1}$  and  $0.165 \text{rad}^2 \text{s}^{-1}$ . Note that this value of  $D_R$  coincides with that extracted from a fit to the theoretical MSD curve<sup>[7f]</sup> and is about 5× smaller compared to the previous reports on AgCl micromotors.<sup>[27]</sup> This  $D_R$  value is also in perfect agreement with the one extracted from the analysis of the MSD data (Figure 2b).

Further, we find a strong dependence of the motion parameters, e.g., MSD and velocity, on the intensity of the blue light (Figure 4; Video S2, Supporting Information). If the intensity of blue light is lower than  $(26 \pm 1) \mu\text{W mm}^{-2}$ , the dynamics of a Janus motor is not distinct from the Brownian fluctuations of a reference particle (under illumination with a green light of low intensity). In this case, the phoretic contribution from the chemical reaction is not sufficiently strong to be discriminated from the Brownian motion, as shown in Figure 4a (switching between green and blue light). Once the intensity of blue light increases, the chemical gradient due to the diffusion of Cl ions around Janus particles becomes larger. This leads to an increase in the speed of Janus particles and a parabolic growth of the corresponding MSD curves in time (Figure 4b). For instance, at blue light illumination with an intensity of  $(106 \pm 1) \mu\text{W mm}^{-2}$ ,

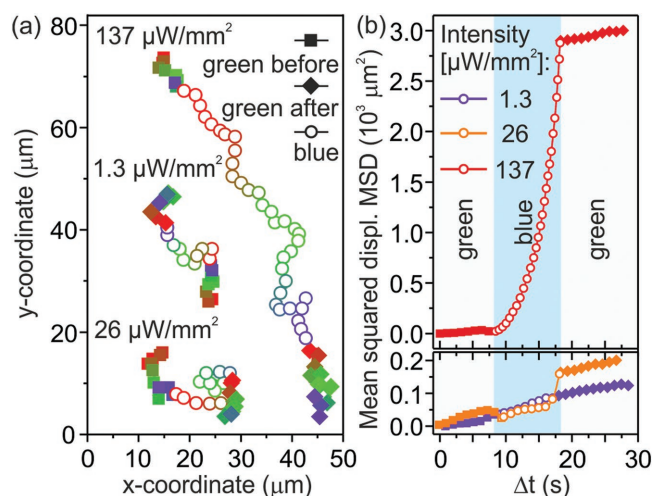


**Figure 4.** a) Trajectories and b) corresponding MSD curves of single Janus PS/Ag/AgCl particles taken over about 27 s when blue light of different intensities [ $(1.3 \pm 1) \mu\text{W mm}^{-2}$ ,  $(26 \pm 1) \mu\text{W mm}^{-2}$ , and  $(137 \pm 1) \mu\text{W mm}^{-2}$ ], on ( $\approx 9$  s), on ( $\approx 9$  s), and off ( $\approx 9$  s) (Video S3, Supporting Information). The intensity of the reference green light is  $(8 \pm 1) \mu\text{W mm}^{-2}$ .

the MSD reaches the value of about  $800 \mu\text{m}^2$  within 8 s (Figures 2b and 3b (experimental data) and Figure 2c (simulation data)), which is 100× higher as compared to the previous visible light-driven Janus BiOI/Au micromotor<sup>[23]</sup> and 7× higher than the reported UV light-driven AgCl micromotors.<sup>[27]</sup> The value of the instantaneous velocity at blue light illumination with an intensity of  $(106 \pm 1) \mu\text{W mm}^{-2}$  reaches  $(7 \pm 2) \mu\text{m s}^{-1}$  (Figure S1, Supporting Information).<sup>[38]</sup> This instantaneous velocity is very similar to the propulsion velocity of about  $5 \mu\text{m s}^{-1}$  extracted from the parabolic fit to the experimental MSD data shown in Figure 2b (for further details we refer to the work by Howse et al.<sup>[7f]</sup>).

## 2.2. Dynamics of Janus Particle Assemblies

Investigations of assemblies of particles were the focus of several works for different passive and active systems.<sup>[19b,26,28,39]</sup> Therefore, it is of interest to analyze the dynamics of assemblies of Ag/AgCl Janus particles. For the novel plasmonic Ag/AgCl Janus spheres realized in this work, in the following we will describe the dynamics of micromotor assemblies of two, three, and clusters consisting of more particles (representative examples of the Janus particle assemblies are shown in Figure 1). The comparison of the motion characteristics of these objects under blue light illumination (blue light intensity of  $(106 \pm 1) \mu\text{W mm}^{-2}$ ) is shown in Figure 5a (Videos S1 and S3, Supporting Information). The tracking of the shown trajectories is done over 12 s, which allows us to plot the MSD for up to 3 s (Figure 5b).

The increase of the number of particles in the cluster leads to a slowdown of the whole assembly (MSD curves in Figure 5b), caused i) by random orientations of the active sides of individual Janus particles within the cluster that suppresses its net velocity, and ii) to a lesser extent, by the suppression of the

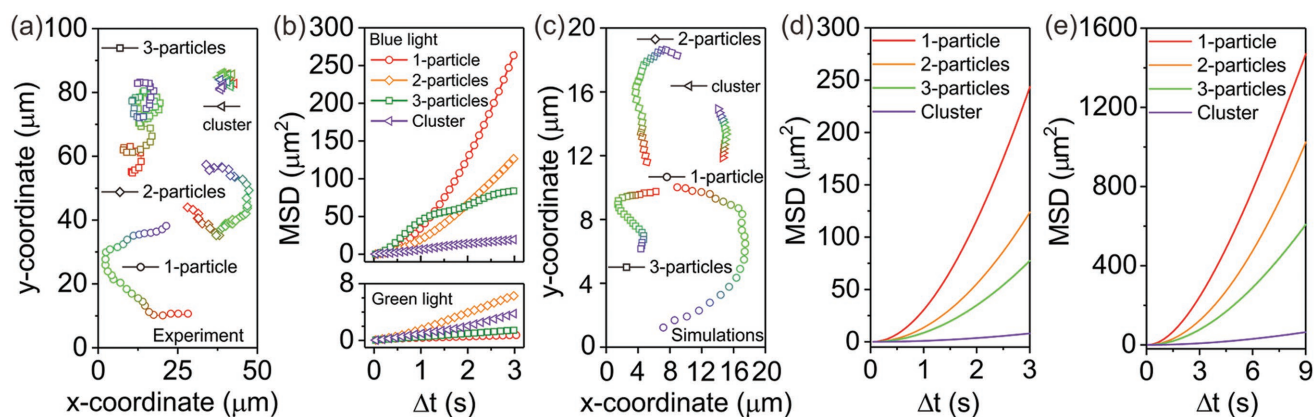


**Figure 5.** a) Trajectories and b) the corresponding experimental MSD curves of different Janus particle assemblies (one, two, three particles, and a cluster consisting of around 30 particles) taken over about 3 s under blue light illumination  $[(106 \pm 1) \mu\text{W mm}^{-2}]$ . c) Simulated trajectories and the corresponding simulated MSD curves for different Janus particle assemblies (one, two, three particles, and a small cluster) taken over d) 3 s and e) 9 s.

translational diffusion of the cluster that scales as  $1/R_{\text{cl}}$ , where  $R_{\text{cl}}$  is the radius of the cluster.

Simulated trajectories and the MSD curves are shown in Figure 5c–e for single, double, triple Janus particles and clusters of many Janus particles. In the case of simulations, we track the motion over a longer time period, of up to 40 s (Figure 5c), which provides a deeper insight into the dynamics of the particle assemblies, e.g., the MSD can be analyzed up to 10 s (Figure 5d). For the sake of comparison with the experimental data (Figure 5a,b), we present a close-up of the theoretical MSD curves for 3 s as well (Figure 5e). The simulation results capture the experimental data rather well. Single Janus particles are characterized by the highest mobility (among single, double, triple particles, and clusters), with self-propelled velocity  $v$  ranging from  $4.75$  to  $6 \mu\text{m s}^{-1}$  (Figure 2c). The corresponding MSD for single Janus particles for  $t = 9$  s varies from  $1100$  to  $2000 \mu\text{m}^2$ , and from  $225$  to  $255 \mu\text{m}^2$  for  $t = 3$  s, which is in good agreement with the experimental values. Assemblies of Janus particles, such as double and triple Janus particles, demonstrate decreasing mobility with the increasing number of constituent particles. This is explained by the random or even antisymmetric orientation of constituent Janus particles in the assemblies when their individual self-velocities are partially cancelled out. As a result, the calculated self-velocities and MSD of double and triple Janus particles are considerably lower:  $v \approx 3.5\text{--}4 \mu\text{m s}^{-1}$ , MSD ( $t = 9$  s)  $\approx 880\text{--}1100 \mu\text{m}^2$  and MSD ( $t = 3$  s)  $\approx 115\text{--}125 \mu\text{m}^2$  (2-particle Janus), and  $v \approx 2.5\text{--}3.5 \mu\text{m s}^{-1}$ , MSD ( $t = 9$  s)  $\approx 425\text{--}650 \mu\text{m}^2$  and MSD ( $t = 3$  s)  $\approx 70\text{--}80 \mu\text{m}^2$  (3-particle Janus). For large clusters of Janus particles these values decrease even further (Figure 2c–e).

In addition to the changes in the self-propelled velocity, the diffusivity of clusters of Janus particles decreases as compared to that of single particles. In the simulations, we used the analytic expressions to estimate the translational  $D_{\text{T}}$  and rotational  $D_{\text{R}}$  diffusion coefficients of the clusters, where  $D_{\text{T}}$  scales as  $1/R_{\text{cl}}$ , and  $D_{\text{R}}$  as  $1/R_{\text{cl}}^3$ . Thus, for 2- and 3-particles, we took  $D_{\text{T}2} = D_{\text{T}}/2$ ,  $D_{\text{R}2} = D_{\text{R}}/8$ , and  $D_{\text{T}3} = D_{\text{T}}/3$ ,  $D_{\text{R}3} = D_{\text{R}}/27$ . For large clusters, where individual particles are closely packed, we evaluated the diffusion coefficients assuming a nearly circular shape of the clusters with a radius that scales with the number

of particles in the cluster  $N_{\text{JPcl}}$  as  $N_{\text{JPcl}}^{1/2}$ . For example, for a cluster with  $N_{\text{JPcl}} = 25$ , the corresponding diffusion coefficients were evaluated as  $D_{\text{Tcl}} = D_{\text{T}}/5$ , and  $D_{\text{Rcl}} = D_{\text{R}}/125$ . From the simulations, it follows that the resulting MSD curves are much less sensitive to variations of the diffusion coefficients than to variations of the self-velocity.

### 2.3. Visible Light Driven Motion in a Physiological Environment

To demonstrate the potential of plasmonic PS/Ag/AgCl-based Janus micromotors for applications in physiological environments, as well as for the applications of environment remediation, we investigate their dynamics in several relevant media under blue light illumination  $[(106 \pm 1) \mu\text{W mm}^{-2}]$  including i) human saliva, ii) PBS, the most common isotonic buffer that mimics the environment of human fluids, and iii) aqueous solution of RhB, which is a typical polluted dye in textile industry. Trajectories and the corresponding MSD of Janus motors composed of 1 particle ( $J_1$ ), 2 particles ( $J_2$ ), and a cluster of many particles ( $J_3$ ) are shown in Figure 6 (Videos S5–S7, Supporting Information). Our experiments reveal that the efficient motion of Janus particles can be detected in 100 times diluted human saliva (Figure 6a),  $0.01 \times 10^{-3}$  M PBS (Figure 6b) and  $100 \times 10^{-3}$  M RhB solution (Figure 6c). Instead, in higher concentrated physiological solutions the motion of PS/Ag/AgCl-based micromotors is highly suppressed, in accordance with the theoretical considerations for the electro kinetic micromotors<sup>[40]</sup> (details in Section 3).

## 3. Discussion

We model the experiments with single Janus particles and their two-, three-, or many-particle assemblies. For the case when there is no asymmetric distribution of chemical products around a Janus particle (reference case of green light illumination in the experiment), Janus particle assemblies undergo Brownian diffusion. Turning blue light ON initiates the chemical reaction leading to a strong radial flow.

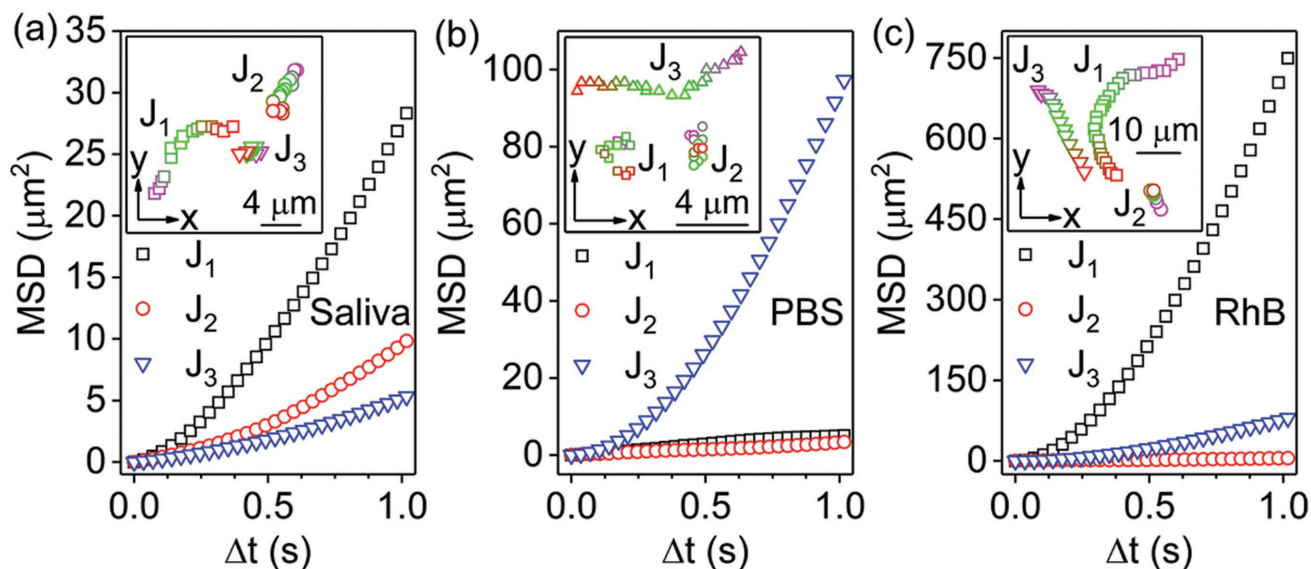


**Figure 6.** Trajectories (insets; taken for 1 s) and the corresponding experimental MSD curves of different Janus particle assemblies ( $J_1$ : single Janus particle;  $J_2$ : 2-particle assembly; and  $J_3$ : big cluster of Janus particles) in a) human saliva solution (100 times diluted) (Video S5, Supporting Information), b) PBS solution ( $0.01 \times 10^{-3} \text{ M}$ ) (Video S6, Supporting Information), and c) RhB solution ( $100 \times 10^{-3} \text{ M}$ ) (Video S7, Supporting Information), under blue light illumination [ $(106 \pm 1) \mu\text{W mm}^{-2}$ ].

A similar set of simulations for clusters consisting of two single Janus particles is presented in Figure S6 (Supporting Information) for seven double Janus particles  $J_{D1}$  to  $J_{D7}$ . Note that since Janus particles in a two-particle configuration are linked by their hydrophobic Ag/AgCl caps (Figure 1e), their resulting self-propelled velocity is always lower than the self-velocity of a single Janus particle:  $v_d < v$ . Our estimates show that the self-propelled velocity of a 2-particle Janus assembly, corresponding to the experimentally measured MSD, can be typically  $v_d \approx 0.5v$  (although  $v_d$  can be very small for “antisymmetric” configurations or close to  $v$  for rare nearly symmetric alignment of Janus particles in a two-particle molecule).

Three-particle clusters of Janus particles (Figure 1d) are generally characterized by similar, or slightly lower, values of self-velocity than two-particle clusters. This is explained by the inside orientation of individual Janus particles by their hydrophobic Ag/AgCl caps, resulting in cancelling out self-velocities of constituent micromotors. Typical values of their self-propelled velocities are estimated to be about  $v_t \approx 0.4v$ . At the same time, three-particle configurations reveal a much stronger ability to rotate, which can be seen in their trajectories shown in Figure S6 (Supporting Information).

Finally, large clusters of Janus particles show even less ability to self-propel, due to the random orientation of individual particles in the clusters. Also, their translational diffusion coefficient scales as  $1/R_{cl}$ , where  $R_{cl}$  is the radius of the cluster. However, this average distance becomes large enough thanks to the strong flow due to the chemical reaction at the surface of many Janus particles in the cluster. Thus, this distance is larger than that for double and triple Janus particles for short times (about 8 s) and is comparable to that for double Janus particles for some longer times. These results agree with the experimental observations.

### 3.1. The Contribution of $v$ and $D_R$ to the Enhanced MSD

The theoretical predicted value of the MSD( $t$ ) of a self-propelled particle,<sup>[7f]</sup> as defined by Equation (1), is mainly determined by the particle self-velocity  $v$  and its rotational diffusion coefficient  $D_R = 1/\tau_R$  and to a much lesser extent by its translational diffusion  $D_T$ , as  $4D_T \ll v^2\tau_R$  for typical experimental conditions. Therefore, the experimentally observed large values of the MSD for Janus particles can be explained by their increased self-propelled velocity  $v$  or by suppressed rotational diffusion, or by both factors together (Figure S6, Supporting Information).

To analyze the effects of the self-velocity and rotational diffusion, we calculated the MSD( $t$ ) for varying self-propelled velocity and the rotational diffusion coefficient  $D_R$ , using Equation (1). First, we fix the rotational diffusion coefficient, which is taken as a theoretical estimate for a  $1 \mu\text{m}$  radius Brownian particle,  $D_R = 0.16 \text{ rad}^2 \text{ s}^{-1}$ , and change the self-propelled velocity. The results are shown in Figure S6b (Supporting Information). The MSD increases from about  $1000 \mu\text{m}^2$  to more than  $2000 \mu\text{m}^2$  for  $t = 10 \text{ s}$  when the self-velocity increases from  $5$  to  $7 \mu\text{m s}^{-1}$ . Note that in numerical simulations, there is a dispersion in the MSD values extracted from trajectories of single Janus particles such that the MSD can reach values as high as  $2000 \mu\text{m}^2$ , for a similar set of parameters (cp. Figure 2c).

To analyze the effect of rotational diffusion, the MSD has been calculated for Janus particles with varying  $D_R$  and fixed self-propelled velocity  $6 \mu\text{m s}^{-1}$  (Figure S6a, Supporting Information). For the reference value of the rotational diffusion coefficient,  $D_R = 0.16 \text{ rad}^2 \text{ s}^{-1}$ , the MSD reaches the value of about  $1600 \mu\text{m}^2$  in 10 s. For the same self-velocity, the MSD increases for decreasing values of  $D_R$ , as shown in Figure S6a (Supporting Information). For example, the measured MSD value of  $3000 \mu\text{m}^2$  can be achieved in 10 s for  $D_R = 0.035 \text{ rad}^2 \text{ s}^{-1}$ , i.e., when the persistence length of the self-propelled motion of

a Janus particle increases about 4.5 times as compared to the estimated theoretical value. In other words, such a considerable increase in the persistence length results in an increase of the MSD value about twice in 10 s. Therefore, for particles characterized by the rotational diffusion coefficient ranging from  $D_R = 0.03$  to  $0.16 \text{ rad}^2 \text{ s}^{-1}$ , for self-velocities in the range of about  $6$  to  $7 \mu\text{m s}^{-1}$ , the MSD values (for 10 s) is in the range of  $1500$ – $3000 \mu\text{m}^2$ , in agreement with the experimentally measured and simulated values (cp. Figure 2).

Early measurements of the MSD of AgCl microparticles illuminated by UV light<sup>[27]</sup> revealed moderate values of the MSD of about  $200 \mu\text{m}^2$ . If we assume that the reason for this considerable change in the MSD (i.e., from  $200$  to  $3000 \mu\text{m}^2$ ) is related to a change in rotational diffusion of the particles, then the rotational diffusion coefficient should be taken about an order of magnitude larger than the reference theoretical value ( $D_R = 0.16 \text{ rad}^2 \text{ s}^{-1}$ ). Namely, the violet MSD curve in Figure S6a (Supporting Information) corresponds to  $D_R = 1.6 \text{ rad}^2 \text{ s}^{-1}$ . The MSD reaches the value of  $226 \mu\text{m}^2$  in 10 s.

This analysis shows that both factors, the increase in the self-propelled velocity and the suppression of rotational diffusion, lead to the detected substantial increase of the MSD of Ag/AgCl Janus particles. Indeed, in our experiments we observe a moderate increase in the self-velocity as compared to previous reports<sup>[38]</sup> and a substantial decrease of the rotational diffusion coefficient as compared to previously reported AgCl micromotors.<sup>[27]</sup>

### 3.2. Motion in Physiological Solutions

The dynamics of micromotors is drastically affected by the physiological liquid and its dilution factors. This is mainly due to the different ionic strengths of the solution and thus screening of the surface charges at the particles. In 1000 times diluted saliva solution, the MSD ( $\Delta t = 1 \text{ s}$ ) of micromotors with 1-, 2-, and a cluster of many Janus particles is measured to be  $3800$ ,  $60$ , and  $490 \mu\text{m}^2$ , respectively (Figure S2b, Supporting Information). But in 10 times diluted saliva solution, the MSD ( $\Delta t = 1 \text{ s}$ ) of micromotors is suppressed to less than  $1.3 \mu\text{m}^2$  (Figure S2d, Supporting Information), which is mainly due to the Brownian motion. A similar trend is also shown in Figure S3b (Supporting Information) for the case when Janus motors move in a  $0.001$  and  $0.1 \times 10^{-3} \text{ M}$  PBS solution. In the case of  $0.001 \times 10^{-3} \text{ M}$  PBS solution, the MSD ( $\Delta t = 1 \text{ s}$ ) of micromotors with 1-, 4-, and a cluster of many Janus particles is  $656$ ,  $100$ , and  $300 \mu\text{m}^2$ , respectively. However, only Brownian motion is observed in  $0.1 \times 10^{-3} \text{ M}$  PBS solution (Figure S3d, Supporting Information). The slowdown and complete stop of the motion in concentrated physiological solutions demonstrate that the mechanism of self-electrodiffusiophoresis is invoked during the motion of Janus PS/Ag/AgCl micromotors.

### 3.3. Wavelength Dependence

Considering the absorption curve (Figure 1k), it is expected that motors should efficiently move even when illuminated using not only blue but also green or red light. Still, similar

to the case with a blue light discussed in this work, proper light intensity is needed to achieve efficient propulsion. As indicated in the Experimental Section, the green light, which we use as a reference, comes directly from a microscope lamp. The light is processed with green and yellow filter sets (hence, it is named here as “green light”) and has very low intensity of  $(8 \pm 1) \mu\text{W mm}^{-2}$ . For comparison, blue light with intensity of  $(106 \pm 1) \mu\text{W mm}^{-2}$  is needed to achieve efficient propulsion of Janus motors. Due to the low intensity of the reference green light, we do not observe an efficient motion of Janus particles. Still, we believe that the reason why Janus particles do not propel efficiently under illumination with the reference green light is its low intensity rather than the wavelength. This assumption is yet to be confirmed experimentally.

### 3.4. Initial Stage of Motion

We note that Janus micromotors do slow down when the exposure time is increased under blue light illumination. Before turning on the blue light lamp, they perform Brownian motion (Figure S4, Supporting Information). Once the blue light lamp is turned on, at the very beginning, the velocity of micromotors rises to  $50 \mu\text{m s}^{-1}$  and then decays down to  $25 \mu\text{m s}^{-1}$  after about 5 s, further maintaining the decreasing trend<sup>[25b]</sup> (Video S8, Supporting Information). Therefore, in this work we focused on the discussion of the trajectories taken after rather long illumination time when the decay of the velocity with time is not pronounced. In this case, we are limited to velocities of about  $7 \mu\text{m s}^{-1}$ .

## 4. Conclusions

We demonstrated, for the first time, the experimental realization and observation of blue light-driven Janus PS/Ag/AgCl micromotors capable of large scale displacements in pure water and the possible usage of them in human saliva, PBS, and RhB solutions. The self-propelled motion is induced by the photocatalytic reaction of Ag/AgCl and its speed can be tuned by changing the light intensity. We showed that a proper design of an Ag/AgCl-based micromotor can boost the MSD to a remarkable value of  $800 \mu\text{m}^2$  in 8 s in pure water, which is about 7 times larger than the MSD values previously reported in the literature for AgCl-based micromotors. The new design employed in our experiments included the following key modifications of the type and the structure of a micromotor: i) Plasmonic Ag/AgCl Janus layer enables efficient visible light ( $>420 \text{ nm}$ ) absorption; ii) heavy AgCl microparticles are replaced by light Janus particles consisting of a  $2 \mu\text{m}$  PS spheres capped with a  $60 \text{ nm}$  thin film of Ag/AgCl; iii) we used a rough capping layer formed by Ag/AgCl nanoparticles, which facilitate the photocatalytic reaction. The high efficiency chemical reaction and the lightness of Janus particles allowed us to achieve high velocities for the Ag/AgCl-based Janus micromotors.

To obtain insight in the dynamics of the newly synthesized Ag/AgCl-based micromotors, we investigated, experimentally and using numerical simulations, the motion of individual Janus particles and their small (consisting of 2 and 3 particles)

and large clusters. The highest velocities of motion and largest MSD values were observed in the case of single Janus particles. With increasing number of particles forming an active “molecule” (consisting of 2 or 3 Janus particles) or a cluster, the detected velocities and MSD decreased, as a result of the cancellation of the self-velocities of the constituent Janus particles due to their random arrangements in the assemblies.

The results of our study bring important insights in the dynamics of these newly synthesized high-motility Ag/AgCl-based micromotors. Our results can be useful for the design of new visible-light-driven high-motility plasmonic photocatalysis micromotors for applications in bioenvironments demanding low toxicity and nondestructive illumination conditions, such as water purification<sup>[27,32a,33,41]</sup> and antibacterial action.<sup>[27,42]</sup>

## 5. Experimental Section

**Materials and Instruments:** All chemicals including the PVP ( $M_w = 55\,000$ ) and iron(III) chloride hexahydrate ( $\text{FeCl}_3 \cdot 6\text{H}_2\text{O}$ ) as well as the polystyrene microparticles (diameters: 1 and 2  $\mu\text{m}$ ) are from Sigma-Aldrich. The 4-wavelength light emitting diode (LED) source and its driver (DC4104) are from THORLABS and the fluorescence lamp (HBO 103) is from Carl Zeiss Microscope. The light power detector (XLP 12) and its monitor are from Gentec-eo. The SEM and EDX were performed in Ultra Plus (Carl Zeiss Microscopy GmbH, Germany) SEM operated at 6 kV and equipped with XFlash QUAD 5060F EDX detector (Bruker Nano GmbH, Germany). The specimens for SEM were prepared by drop casting a 2  $\mu\text{L}$  microparticle solution on a 5 mm  $\times$  5 mm Si wafer and coating it with a 20 nm carbon (SCD500 coater, Leica Microsystems GmbH, Germany) to reduce the charging of the specimen in the electron beam. The UV-vis spectra are measured by a UV-vis Spectrometer (Varian Cary 50 Bio). The pH values of physiological solutions are measured by a pH meter (InoLab Terminal Level 3, WTW GmbH).

**Fabrication of Janus Silver Chloride Coated Polystyrene Microparticles (Janus PS@Ag/AgCl):** Monolayers of 2  $\mu\text{m}$  PS particles (Sigma-Aldrich) were prepared by drop casting the PS ethanol suspension (25 mg mL<sup>-1</sup>) onto glass slides preprocessed by a plasma activation equipment. A 60 nm thin Ag layer was deposited on the top surface of the monolayer using electron beam deposition (base pressure:  $7 \times 10^{-7}$  mbar; deposition rate is 1 nm s<sup>-1</sup>). To detach the capped particles from the glass slides, sonication processing for 15 min was applied. The Janus Ag coated polystyrene particles (PS/Ag) were collected and resuspended in DI water. The Janus Ag/AgCl coated polystyrene particles (PS/Ag/AgCl) were synthesized following the established procedure.<sup>[32b,33]</sup> In brief, Janus PS/Ag particles were dispersed in a PVP solution ( $50 \times 10^{-3}$  M). Then, an excess  $\text{FeCl}_3$  solution (0.02 M) was added to the initial solution in a dark environment. After 20 min of stirring, the solution was centrifuged and the resulting Janus PS/Ag/AgCl were decanted and resuspended in DI water five times to remove the  $\text{FeCl}_3$  and PVP from the solution. The Janus PS/Ag/AgCl particles were kept suspended in DI water and stored in a fridge for future use. The whole synthesis process must be done in a dark environment.

**Optical Video Recording:** The motion of Janus PS/Ag/AgCl particles and 1  $\mu\text{m}$  tracer was recorded with a Carl Zeiss inverted microscope (Axiovert 200 M) integrated with a Cascade video camera (5120), a 20 $\times$  air and a 100 $\times$  oil transmitted-light objectives. The suspension with Janus micromotors was diluted and mixed on a clean glass slide with a droplet of DI water. To study the collective behavior, a suspension with PS beads was dispersed in a DI water droplet and then it was further diluted in the suspension with Janus PS/Ag/AgCl particles. 400 frames video files were recorded with a Cascade camera at a frame rate of 28 frames per second.

**Green Light Illumination:** For reference measurements, we used light which directly comes from the microscope lamp (12 V and 100 W

Halogen lamp) and is processed with green and yellow filter sets. The green light intensity is  $(8 \pm 1) \mu\text{W mm}^{-2}$ .

**Blue Light Illumination:** For the experiment which shows Janus particles under different intensity blue lights, we use the 4-wavelength LED source to selectively provide 490 nm blue light with  $(1.3 \pm 0.2) \mu\text{W mm}^{-2}$ ,  $(26 \pm 1) \mu\text{W mm}^{-2}$ , and  $(137 \pm 1) \mu\text{W mm}^{-2}$  intensities. The blue light source for the other experiments was provided by the external fluorescence lamp with Zeiss filter set (excitation with BP 450–490 nm and emission with LP 515 nm,  $(106 \pm 1) \mu\text{W mm}^{-2}$ ) and it can be controlled with on/off modes by opening or closing the shutter. All the light intensities were measured with a light power detector (gentec-eo XLP 12).

**Video Analysis:** Custom scripts in Python using the OpenCV library<sup>[3c]</sup> and TrackMate<sup>[43]</sup> from the image processing software Fiji (<http://fiji.sc/>) were used for particle tracking to obtain the trajectory data of Janus PS/Ag/AgCl particles and their assemblies. A custom MATLAB script was written to analyze the trajectory data, utilizing the per-value class @msdanalyzer (<https://tinevez.github.io/msdanalyzer/>) to calculate the MSD, instantaneous velocity, and the radial displacement of Janus particles. The MSD was calculated as follows:  $\text{MSD} = [r(t + \Delta t) - r(t)]^2$ , with  $\Delta t$  the time step between video frames and  $r$  the  $(x, y)$  coordinate values from individual video tracking.<sup>[44]</sup> The MSAD was calculated following the established method:  $\text{MSAD} = [(\theta(t + \Delta t) - \theta(t))^2]$ . This value is used to calculate the  $D_R$ .  $D_R = \text{MSAD}/(2\Delta t)$ . The angular autocorrelation is calculated using the equation  $\cos[(\theta(t + \Delta t) - \theta(t))_{(t=0)}]$ .<sup>[3c]</sup>

**Impact of Thermophoresis:** To investigate a possible contribution from thermophoresis, we prepared reference 2  $\mu\text{m}$  Janus particles coated with only a 60 nm thin Ag layer and analyzed the MSD data with blue light off and on. The MSDs of a single Janus PS/Ag particle are 9.5 and 13  $\mu\text{m}^2$  after 1 s when illuminating without/with blue light, respectively (Figure S5 and Video S4, Supporting Information). These figures are way smaller compared to the case of Janus PS/Ag/AgCl particles. Hence, thermophoresis can be safely excluded as the main driving mechanism. The slight increase of MSD under blue light is due to the enhanced absorption of the blue light and resulting heating effect.<sup>[1]6a,c]</sup>

**Simulations:** The motion of active micromotors characterized by self-propelled velocity  $v$  was simulated by numerically integrating the following overdamped Langevin equations<sup>[30b-d]</sup>

$$\begin{aligned}\dot{x}_i &= v_0 \cos \theta_i + \xi_{i0,x}(t) + \mu \sum_{ij}^N f_{ij,x} \\ \dot{y}_i &= v_0 \sin \theta_i + \xi_{i0,y}(t) + \mu \sum_{ij}^N f_{ij,y} \\ \dot{\theta} &= \xi_{i\theta}(t)\end{aligned}\quad (3)$$

for  $ij$  running from 1 to the total number  $N$  of particles, active and passive, in the system. Here  $\mu$  is the mobility of Janus particles,  $\xi_{i0}(t) = (\xi_{i0,x}(t), \xi_{i0,y}(t))$  is a 2D thermal Gaussian noise with correlation functions  $\langle \xi_{0,\alpha}(t) \rangle = 0$ ,  $\langle \xi_{0,\alpha}(t) \xi_{0,\beta}(t) \rangle = 2D_T \xi_{\alpha\beta} \delta(t)$ , where  $\alpha, \beta = x, y$ , and  $D_T$  is the translational diffusion constant of a passive particle of the same geometry as an active micromotor, at a fixed temperature;  $\xi_{i\theta}(t)$  is an independent 1D Gaussian noise with correlation functions  $\langle \xi_{i\theta}(t) \rangle = 0$  and  $\langle \xi_{i\theta}(t) \xi_{i\theta}(0) \rangle = 2D_R \delta(t)$  that models the fluctuations of the propulsion angle  $\theta$ . The diffusion coefficients  $D_T$  and  $D_R$  can be directly calculated<sup>[45]</sup> or extracted from experimentally measured trajectories and MSD. Thus, for a particle with radius  $R_p = 1 \mu\text{m}$  diffusing in water at room temperature, the corresponding translational diffusion coefficient is  $D_T \approx 0.22 \mu\text{m}^2 \text{s}^{-1}$ , and the rotational diffusion coefficient is  $D_R \approx 0.16 \text{rad}^2 \text{s}^{-1}$ .<sup>[37]</sup>

## Supporting Information

Supporting Information is available from the Wiley Online Library or from the author.

## Acknowledgements

The authors thank N. Pütz (TU Dresden) for support with the SEM measurements, B. Ibarlucea (TU Dresden) for Zeta potential measurements, J. Grenzer and A. Scholz (HZDR) for X-ray diffraction characterization. Support by the Nanofabrication Facilities Rossendorf and Structural Characterization Facilities Rossendorf at the Ion Beam Center (IBC) at the HZDR is greatly appreciated. D.M., X.W., and L.B. formulated the task. X.W. carried out experimental work with the contribution from A.N., J.G., T.H., and L.B. P.F. performed the SEM and EDX analysis. V.R.M. performed simulations and analyzed the data with the contribution from J.T. and F.N. The manuscript was written by D.M., L.B., and V.R.M. with the contribution from X.W., J.G., A.N., G.C., J.F., J.T., and F.N. All authors have given approval to the final version of the manuscript. The work was financially supported in part via the German Science Foundation (DFG) Grant MA 5144/9-1, BA 4986/7-1 and the European Research Council under the European Union's Seventh Framework Programme (FP7/2007-2013)/ERC grant agreement no. 306277. V.R.M. and F.N. acknowledge support by the Research Foundation–Flanders (FWO-VI) and Japan Society for the Promotion of Science (JSPS) (JSPS-FWO Grant No. VS.059.18N). F.N. was partially supported by the MURI Center for Dynamic Magneto-Optics via the Air Force Office of Scientific Research (AFOSR) (FA9550-14-1-0040), Army Research Office (ARO) (Grant No. 73315PH), Asian Office of Aerospace Research and Development (AOARD) (Grant No. FA2386-18-1-4045), Japan Science and Technology Agency (JST) (the ImPACT program and CREST Grant No. JPMJCR1676), Japan Society for the Promotion of Science (JSPS) (JSPS-RFBR Grant No. 17-52-50023), RIKEN-AIST Challenge Research Fund, and the John Templeton Foundation.

## Conflict of Interest

The authors declare no conflict of interest.

## Keywords

active Janus particles, fuel-free micromotors, plasmonic photoreaction, visible light

Received: September 4, 2018  
Published online:

- [1] a) J. Wang, *ACS Nano* **2009**, *3*, 4; b) S. Sengupta, M. E. Ibele, A. Sen, *Angew. Chem., Int. Ed.* **2012**, *51*, 8434; c) P. Illien, R. Golestanian, A. Sen, *Chem. Soc. Rev.* **2017**, *46*, 5508; d) J. L. Moran, J. D. Posner, *Annu. Rev. Fluid Mech.* **2017**, *49*, 511; e) J. Zhang, E. Luijten, B. A. Grzybowski, S. Granick, *Chem. Soc. Rev.* **2017**, *46*, 5551.
- [2] a) H. Wang, M. Pumera, *Chem. Rev.* **2015**, *115*, 8704; b) W. Gao, J. Wang, *ACS Nano* **2014**, *8*, 3170; c) M. Guix, C. C. Mayorga-Martinez, A. Merkoçi, *Chem. Rev.* **2014**, *114*, 6285.
- [3] a) Z. Wu, Y. Wu, W. He, X. Lin, J. Sun, Q. He, *Angew. Chem., Int. Ed.* **2013**, *52*, 7000; b) W. Gao, R. Dong, S. Thamphiwatana, J. Li, W. Gao, L. Zhang, J. Wang, *ACS Nano* **2015**, *9*, 117; c) X. Ma, A. C. Hortelao, A. Miguel-Lopez, S. Sanchez, *J. Am. Chem. Soc.* **2016**, *138*, 13782.
- [4] a) S. Tottori, L. Zhang, F. Qiu, K. K. Krawczyk, A. Franco-Obregón, B. J. Nelson, *Adv. Mater.* **2012**, *24*, 811; b) D. Schamel, M. Pfeifer, J. G. Gibbs, B. Miksch, A. G. Mark, P. Fischer, *J. Am. Chem. Soc.* **2013**, *135*, 12353.
- [5] a) C. Maggi, F. Saglimbeni, M. Dipalo, F. De Angelis, R. Di Leonardo, *Nat. Commun.* **2015**, *6*, 7855; b) M. Yang, M. Ripoll, *Soft Matter* **2014**, *10*, 1006.
- [6] a) W. F. Paxton, K. C. Kistler, C. C. Olmeda, A. Sen, S. K. St Angelo, Y. Cao, T. E. Mallouk, P. E. Lammert, V. H. Crespi, *J. Am. Chem. Soc.* **2004**, *126*, 13424; b) S. Sattayasamitsathit, W. Gao, P. Calvo-Marzal, K. M. Manesh, J. Wang, *ChemPhysChem* **2010**, *11*, 2802.
- [7] a) L. Baraban, M. Tasinkevych, M. N. Popescu, S. Sanchez, S. Dietrich, O. G. Schmidt, *Soft Matter* **2012**, *8*, 48; b) W. Gao, A. Pei, R. Dong, J. Wang, *J. Am. Chem. Soc.* **2014**, *136*, 2276; c) X. Ma, K. Hahn, S. Sanchez, *J. Am. Chem. Soc.* **2015**, *137*, 4976; d) X. Ma, S. Jang, M. N. Popescu, W. E. Uspal, A. Miguel-López, K. Hahn, D.-P. Kim, S. Sánchez, *ACS Nano* **2016**, *10*, 8751; e) B. Jang, A. Hong, H. E. Kang, C. Alcantara, S. Charreyron, F. Mushtaq, E. Pellicer, R. Buchel, J. Sort, S. S. Lee, B. J. Nelson, S. Pane, *ACS Nano* **2017**, *11*, 6146; f) J. R. Howse, R. A. L. Jones, A. J. Ryan, T. Gough, R. Vafabakhsh, R. Golestanian, *Phys. Rev. Lett.* **2007**, *99*, 048102; g) L. Baraban, D. Makarov, R. Streubel, I. Mönch, D. Grimm, S. Sanchez, O. G. Schmidt, *ACS Nano* **2012**, *6*, 3383; h) L. Baraban, D. Makarov, O. G. Schmidt, G. Cuniberti, P. Leiderer, A. Erbe, *Nanoscale* **2013**, *5*, 1332; i) L. Baraban, S. M. Harazim, S. Sánchez, O. G. Schmidt, *Angew. Chem., Int. Ed.* **2013**, *52*, 5552.
- [8] J. Katuri, X. Ma, M. M. Stanton, S. Sánchez, *Acc. Chem. Res.* **2017**, *50*, 2.
- [9] a) W. Gao, J. Wang, *Nanoscale* **2014**, *6*, 10486; b) J. Li, B. E.-F. de Ávila, W. Gao, L. Zhang, J. Wang, *Sci. Rob.* **2017**, *2*, eaam6431; c) F. Peng, Y. Tu, D. A. Wilson, *Chem. Soc. Rev.* **2017**, *46*, 5289; d) W. Gao, S. Sattayasamitsathit, J. Orozco, J. Wang, *J. Am. Chem. Soc.* **2011**, *133*, 11862.
- [10] a) A. A. Solovev, Y. Mei, E. Bermúdez Ureña, G. Huang, O. G. Schmidt, *Small* **2009**, *5*, 1688; b) H. Wang, G. Zhao, M. Pumera, *J. Am. Chem. Soc.* **2014**, *136*, 2719; c) J. Li, X. Yu, M. Xu, W. Liu, E. Sandraz, H. Lan, J. Wang, S. M. Cohen, *J. Am. Chem. Soc.* **2017**, *139*, 611.
- [11] a) W. F. Paxton, P. T. Baker, T. R. Kline, Y. Wang, T. E. Mallouk, A. Sen, *J. Am. Chem. Soc.* **2006**, *128*, 14881; b) U. K. Demirok, R. Laocharoensuk, K. M. Manesh, J. Wang, *Angew. Chem., Int. Ed.* **2008**, *47*, 9349; c) R. Liu, A. Sen, *J. Am. Chem. Soc.* **2011**, *133*, 20064; d) F. Wong, A. Sen, *ACS Nano* **2016**, *10*, 7172.
- [12] a) W. Wang, L. A. Castro, M. Hoyos, T. E. Mallouk, *ACS Nano* **2012**, *6*, 6122; b) V. Garcia-Gradilla, J. Orozco, S. Sattayasamitsathit, F. Soto, F. Kuralay, A. Pourazary, A. Katzenberg, W. Gao, Y. Shen, J. Wang, *ACS Nano* **2013**, *7*, 9232.
- [13] a) R. Dreyfus, J. Baudry, M. L. Roper, M. Fermigier, *Nature* **2005**, *437*, 862; b) A. Ghosh, P. Fischer, *Nano Lett.* **2009**, *9*, 2243; c) B. Jang, E. Gutman, N. Stucki, B. F. Seitz, P. D. Wendel-García, T. Newton, J. Pokki, O. Ergeneman, S. Pané, Y. Or, *Nano Lett.* **2015**, *15*, 4829; d) F. M. Qiu, S. Fujita, R. Mhanna, L. Zhang, B. R. Simona, B. J. Nelson, *Adv. Funct. Mater.* **2015**, *25*, 1666; e) X. Z. Chen, M. Hoop, N. Shamsudhin, T. Huang, B. Ozkale, Q. Li, E. Siringil, F. Mushtaq, L. Di Tizio, B. J. Nelson, S. Pane, *Adv. Mater.* **2017**, *29*, 1605458; f) T. Li, J. Li, K. I. Morozov, Z. Wu, T. Xu, I. Rozen, A. M. Leshansky, L. Li, J. Wang, *Nano Lett.* **2017**, *17*, 5092; g) X. Yan, Q. Zhou, M. Vincent, Y. Deng, J. Yu, J. Xu, T. Xu, T. Tang, L. Bian, Y.-X. J. Wang, K. Kostarelos, L. Zhang, *Sci. Rob.* **2017**, *2*, eaaq1155.
- [14] a) W. Wang, W. Duan, S. Ahmed, A. Sen, T. E. Mallouk, *Acc. Chem. Res.* **2015**, *48*, 1938; b) D. Velegol, A. Garg, R. Guha, A. Kar, M. Kumar, *Soft Matter* **2016**, *12*, 4686.
- [15] a) Y. F. Tu, F. Peng, D. A. Wilson, *Adv. Mater.* **2017**, *29*, 1701970; b) L. Xu, F. Mou, H. Gong, M. Luo, J. Guan, *Chem. Soc. Rev.* **2017**, *46*, 6905.
- [16] a) H.-R. Jiang, N. Yoshinaga, M. Sano, *Phys. Rev. Lett.* **2010**, *105*, 268302; b) L. Baraban, R. Streubel, D. Makarov, L. Han, D. Karnauschenko, O. G. Schmidt, G. Cuniberti, *ACS Nano* **2013**, *7*, 1360; c) L. Helden, R. Eichhorn, C. Bechinger, *Soft Matter* **2015**, *11*, 2379.
- [17] a) R. Dong, Q. Zhang, W. Gao, A. Pei, B. Ren, *ACS Nano* **2016**, *10*, 839; b) Z. Lin, T. Si, Z. Wu, C. Gao, X. Lin, Q. He, *Angew. Chem.,*

- Int. Ed.* **2017**, *56*, 13517; c) D. Zhou, L. Ren, Y. C. Li, P. Xu, Y. Gao, G. Zhang, W. Wang, T. E. Mallouk, L. Li, *Chem. Commun.* **2017**, *53*, 11465.
- [18] a) Z. Wu, X. Lin, Y. Wu, T. Si, J. Sun, Q. He, *ACS Nano* **2014**, *8*, 6097; b) J. Shao, M. Xuan, L. Dai, T. Si, J. Li, Q. He, *Angew. Chem., Int. Ed.* **2015**, *54*, 12782; c) M. Xuan, Z. Wu, J. Shao, L. Dai, T. Si, Q. He, *J. Am. Chem. Soc.* **2016**, *138*, 6492.
- [19] a) M. Ibele, T. E. Mallouk, A. Sen, *Angew. Chem., Int. Ed.* **2009**, *48*, 3308; b) Y. Hong, M. Diaz, U. M. Córdoba-Figueroa, A. Sen, *Adv. Funct. Mater.* **2010**, *20*, 1568; c) B. Dai, J. Wang, Z. Xiong, X. Zhan, W. Dai, C. C. Li, S. P. Feng, J. Tang, *Nat. Nanotechnol.* **2016**, *11*, 1087; d) C. Chen, F. Mou, L. Xu, S. Wang, J. Guan, Z. Feng, Q. Wang, L. Kong, W. Li, J. Wang, Q. Zhang, *Adv. Mater.* **2017**, *29*, 1603374; e) R. Dong, C. Wang, Q. Wang, A. Pei, X. She, Y. Zhang, Y. Cai, *Nanoscale* **2017**, *9*, 15027; f) D. P. Singh, U. Choudhury, P. Fischer, A. G. Mark, *Adv. Mater.* **2017**, *29*, 1701328.
- [20] K. König, Y. Tadir, P. Patrizio, M. W. Berns, B. J. Tromberg, *Hum. Reprod.* **1996**, *11*, 2162.
- [21] X. Wang, V. Sridhar, S. Guo, N. Talebi, A. Miguel-López, K. Hahn, P. A. van Aken, S. Sánchez, *Adv. Funct. Mater.* **2018**, *28*, 1705862.
- [22] a) J. Wang, Z. Xiong, X. Zhan, B. Dai, J. Zheng, J. Liu, J. Tang, *Adv. Mater.* **2017**, *29*, 1701451; b) D. Zhou, Y. C. Li, P. Xu, N. S. McCool, L. Li, W. Wang, T. E. Mallouk, *Nanoscale* **2017**, *9*, 75.
- [23] R. Dong, Y. Hu, Y. Wu, W. Gao, B. Ren, Q. Wang, Y. Cai, *J. Am. Chem. Soc.* **2017**, *139*, 1722.
- [24] D. Zhou, Y. C. Li, P. Xu, L. Ren, G. Zhang, T. E. Mallouk, L. Li, *Nanoscale* **2017**, *9*, 11434.
- [25] a) P. Wang, B. B. Huang, X. Y. Qin, X. Y. Zhang, Y. Dai, J. Y. Wei, M. H. Whangbo, *Angew. Chem., Int. Ed.* **2008**, *47*, 7931; b) C. Zhou, H. P. Zhang, J. Y. Tang, W. Wang, *Langmuir* **2018**, *34*, 3289.
- [26] M. E. Ibele, P. E. Lammert, V. H. Crespi, A. Sen, *ACS Nano* **2010**, *4*, 4845.
- [27] J. Simmchen, A. Baeza, A. Miguel-Lopez, M. M. Stanton, M. Vallet-Regí, D. Ruiz-Molina, S. Sanchez, *ChemNanoMat* **2017**, *3*, 65.
- [28] A. Altemose, M. A. Sanchez-Farran, W. Duan, S. Schulz, A. Borhan, V. H. Crespi, A. Sen, *Angew. Chem., Int. Ed.* **2017**, *56*, 7817.
- [29] a) W. Hou, S. B. Cronin, *Adv. Funct. Mater.* **2013**, *23*, 1612; b) Z. W. Seh, S. Liu, M. Low, S. Y. Zhang, Z. Liu, A. Mlayah, M. Y. Han, *Adv. Mater.* **2012**, *24*, 2310; c) K. Awazu, M. Fujimaki, C. Rockstuhl, J. Tominaga, H. Murakami, Y. Ohki, N. Yoshida, T. Watanabe, *J. Am. Chem. Soc.* **2008**, *130*, 1676; d) Z. Liu, W. Hou, P. Pavaskar, M. Aykol, S. B. Cronin, *Nano Lett.* **2011**, *11*, 1111; e) S. Linic, P. Christopher, D. B. Ingram, *Nat. Mater.* **2011**, *10*, 911; f) Y. X. Tang, Z. L. Jiang, G. C. Xing, A. R. Li, P. D. Kanhere, Y. Y. Zhang, T. C. Sum, S. Z. Li, X. D. Chen, Z. L. Dong, Z. Chen, *Adv. Funct. Mater.* **2013**, *23*, 2932.
- [30] a) Y. Fily, M. C. Marchetti, *Phys. Rev. Lett.* **2012**, *108*, 235702; b) P. K. Ghosh, V. R. Misko, F. Marchesoni, F. Nori, *Phys. Rev. Lett.* **2013**, *110*, 268301; c) D. Takagi, A. B. Braunschweig, J. Zhang, M. J. Shelley, *Phys. Rev. Lett.* **2013**, *110*, 038301; d) H. Yu, A. Kopach, V. R. Misko, A. A. Vasylenko, D. Makarov, F. Marchesoni, F. Nori, L. Baraban, G. Cuniberti, *Small* **2016**, *12*, 5882.
- [31] S. Glaus, G. Calzaferri, *Photochem. Photobiol. Sci.* **2003**, *2*, 398.
- [32] a) C. An, S. Peng, Y. Sun, *Adv. Mater.* **2010**, *22*, 2570; b) Y. Bi, J. Ye, *Chem. Commun.* **2009**, 6551; c) P. Wang, B. Huang, Z. Lou, X. Zhang, X. Qin, Y. Dai, Z. Zheng, X. Wang, *Chem. - Eur. J.* **2010**, *16*, 538; d) T. B. Devi, S. Begum, M. Ahmaruzzaman, *J. Photochem. Photobiol., B* **2016**, *160*, 260; e) Y. Qin, Y. Cui, Z. Tian, Y. Wu, Y. Li, *Nanoscale Res. Lett.* **2017**, *12*, 247.
- [33] J. Ge, X. Wang, H. B. Yao, H. W. Zhu, Y. C. Peng, S. H. Yu, *Mater. Horiz.* **2015**, *2*, 509.
- [34] S. Zhang, J. Li, X. Wang, Y. Huang, M. Zeng, J. Xu, *ACS Appl. Mater. Interfaces* **2014**, *6*, 22116.
- [35] G. Calzaferri, *Catal. Today* **1997**, *39*, 145.
- [36] a) M. J. Saxton, *Biophys. J.* **1997**, *72*, 1744; b) O. Chiarelli-Neto, A. S. Ferreira, W. K. Martins, C. Pavani, D. Severino, F. Faiao-Flores, S. S. Maria-Engler, E. Aliprandini, G. R. Martinez, P. Di Mascio, M. H. Medeiros, M. S. Baptista, *PLoS One* **2014**, *9*, e113266.
- [37] G. Volpe, S. Gigan, G. Volpe, *Am. J. Phys.* **2014**, *82*, 659.
- [38] J. Zheng, B. Dai, J. Wang, Z. Xiong, Y. Yang, J. Liu, X. Zhan, Z. Wan, J. Tang, *Nat. Commun.* **2017**, *8*, 1438.
- [39] a) W. Duan, R. Liu, A. Sen, *J. Am. Chem. Soc.* **2013**, *135*, 1280; b) J. Palacci, S. Sacanna, A. P. Steinberg, D. J. Pine, P. M. Chaikin, *Science* **2013**, *339*, 936.
- [40] A. T. Brown, W. C. K. Poon, C. Holm, J. de Graaf, *Soft Matter* **2017**, *13*, 1200.
- [41] a) M. Zhu, P. Chen, M. Liu, *ACS Nano* **2011**, *5*, 4529; b) H. Zhang, X. Fan, X. Quan, S. Chen, H. Yu, *Environ. Sci. Technol.* **2011**, *45*, 5731; c) Y. S. Yang, Y. Zhang, M. G. Dong, T. Yan, M. S. Zhang, Q. R. Zeng, *J. Hazard. Mater.* **2017**, *335*, 92.
- [42] D. Vilela, M. M. Stanton, J. Parmar, S. Sanchez, *ACS Appl. Mater. Interfaces* **2017**, *9*, 22093.
- [43] K. Jaqaman, D. Loerke, M. Mettlen, H. Kuwata, S. Grinstein, S. L. Schmid, G. Danuser, *Nat. Methods* **2008**, *5*, 695.
- [44] a) G. Dunderdale, S. Ebbens, P. Fairclough, J. Howse, *Langmuir* **2012**, *28*, 10997; b) L. Weimann, K. A. Ganzinger, J. McColl, K. L. Irvine, S. J. Davis, N. J. Gay, C. E. Bryant, D. Klenerman, *PLoS One* **2013**, *8*, e64287.
- [45] E. Purcell, *Am. J. Phys.* **1977**, *45*, 3.